JOURNAL OF MATERIALS SCIENCE 31 (1996) 1285–1294

A microstructural study of fibre/mortar interfaces during fibre debonding and pull-out

Y. GENG, C. K. Y. LEUNG
Department of Civil and Environmental Engineering, Massachusetts Institute of Technology, Cambridge, MA 02139, USA

Attempts were made to connect the change in interfacial properties during fibre pull-out in cementitious material to the microstructural features of the interface. The microstructural features of fibre (steel, nylon and polypropylene)/mortar interfaces were examined during the fibre debonding and pull-out process. Because fibre pull-out was found to be sensitive to lateral compression, microscopic studies were carried out on fibres pulled out with and without lateral compression. SEM and energy-dispersive X-ray (EDX) analyses were performed at four different stages: (a) before debonding; (b) immediately after debonding; (c) at small sliding distance; and (d) at large sliding distance. For the steel fibre/mortar interface, it was found that the mortar surface (interfacial transition zone) was subjected to abrasion, while the steel surface was subjected to plastic deformation. EDX analysis on the mortar interface showed that the ratio of calcium/silicon count first increases within a short sliding distance and decreases thereafter, indicating a process of CH layer abrasion and C–S–H layer exposure. The rapid post-peak drop of the pull-out force at the beginning of sliding is due to the "grinding" effect, which leads to crushing and abrasion of the CH crystals and a reduction of asperity on the mortar surface. The grinding and abrasion effect becomes more significant with the application of lateral compression, which results in more rapid drop of the pullout force. For the nylon and polypropylene fibre/mortar interfaces, the fibre surface peels and the mortar surface experiences very little damage. Nylon fibre surface swells and is peeled with short whiskers on the surface, leading to significant increase in interfacial friction causing the post-debonding pull-out force to increase. The polypropylene fibre surface is peeled and plowed with long whiskers and long scratch lines which also leads to an increase in interfacial friction. On applying lateral compression to the mortar during fibre pull-out, the abrasion and peeling effects are more severe. With lateral compression, holes may form on the polypropylene surface over a longer sliding distance. The ratio of calcium/silicon count on the mortar surface by EDX does not show obvious trends with sliding distance indicating that the mortar surface experiences very little damage.

1. Introduction

The performance of fibre-reinforced concrete (FRC) is strongly affected by the fibre debonding/pull-out behaviour [1–3]. For different fibres, the pull-out curves may exhibit totally different trends. For example, the interfacial friction, which is very sensitive to interfacial microstructures, may either decrease rapidly (steel FRC [4, 5]) or increase slightly (polymeric FRC [6]) after total debonding. In order to understand the variation of interfacial friction during fibre debonding and pull-out, it is necessary to investigate microstructural features at the interface, especially the damage evolution of the microstructure during fibre pull-out.

1.1. Steel fibre/concrete interface

It has been found that the microstructure near the cement paste, mortar or concrete interface is considerably different from the bulk matrix [7–11]. An SEM study by Bentur *et al.* [10] concluded that the interfacial zone around steel fibres can be characterized by several layers (Fig. 1). The steel fibre surface is in contact with a thin duplex film layer (1 μm) consisting of a sub-layer of CH next to the steel and a C–S–H sub-layer. More than half of the area outside this duplex film is occupied by a thicker layer of dense CH crystals which is about 10–20 μm thick. The remaining area scattered among the dense CH crystals is a porous zone that contains some C–S–H gel and possibly some ettringite particles (AFt, calcium aluminium trisulphate). Around the thick CH layer is a distinct porous layer of C–S–H gel, and only beyond that porous layer is the bulk cement paste microstructure observed. The region surrounding the fibre thus contains a very porous and weak layer parallel to the fibre which extends at least 10 μm from the fibre surface.

0022–2461

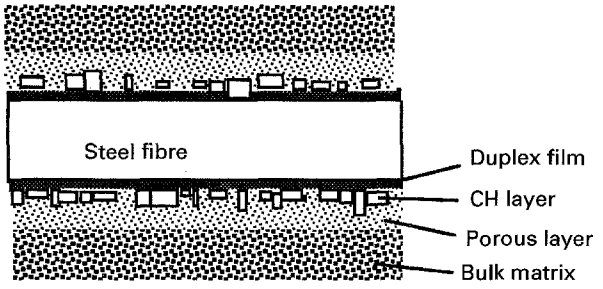

Figure 1 Microstructure of the steel fibre/cement interface [10].

Although the microstructure of the fibre/mortar interface is reasonably well understood, the microstructural change of interface during the fibre pull-out process, due to interfacial debonding and frictional wear, are known in considerably less detail. To the author's knowledge, only Pinchin and Tabor [12] have attempted to explain the decrease in interfacial friction of steel fibre/mortar during the pull-out process based on the surface compaction of hydrated cement paste observed by Soroka and Sereda [13].

Pinchin and Tabor attributed the significant friction decrease during a small amount of steel fibre pull-out to densification or compaction, but not to wear, on the mortar surface. They argued that the compaction during fibre pull-out occurs on a very fine scale of the order of 0.1–0.3 μm near the embedded steel fibre and is difficult to detect. Because their conclusions are based on the final stage of the pull-out test, i.e. at total fibre pull-out, it does not reflect the whole pull-out process.

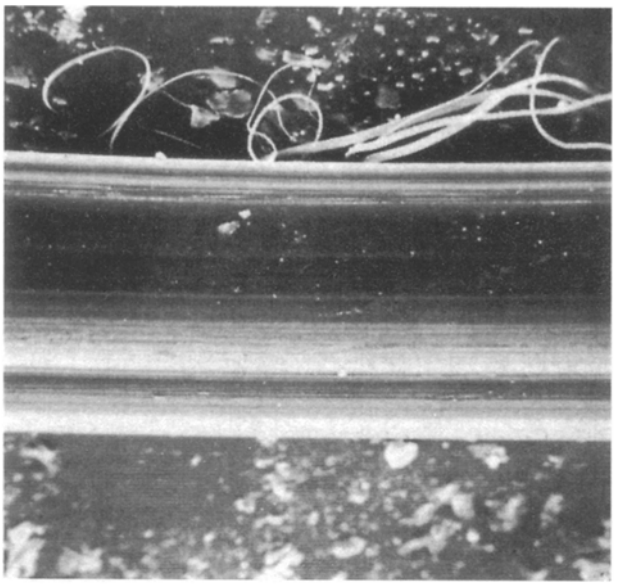

Figure 2 Shaving on polypropylene fibre (diameter $d = 340$ μm) [16].

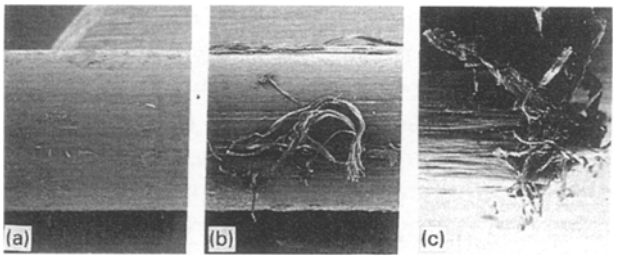

Figure 3 Peeling and fibrillation on nylon fibre ($d = 500$ μm, s = slippage distance) [6].

1.2. Polymeric fibre/concrete interface

A few researchers [6, 14–18] have studied polymeric FRCs. Polymeric fibres have high yield strength, but unlike steel fibre, they have lower elastic moduli and transverse strengths than cementitious materials. Therefore, the interfacial damage mechanism of polymeric fibre/mortar is different from that of steel fibre/mortar. Polymeric fibres also have less corrosion in harsh environment, but high creeping effect. Based on these properties, polymeric fibres have been used to reinforce FRC in the early stage when the matrix is weak, and of low modulus, or to resist impact load and eliminate corrosion.

Polypropylene fibre was the first polymeric fibre applied to concrete in forms of monofilament or fibrillated film. Baggott and Gandhi [16] studied continuous monofilament polypropylene fibre (340 μm) reinforced cement beam under tensile load. They observed defects of up to 10 μm in size on the polypropylene fibre interface. One typical type of damage observed was the chiselling out of a long shaving of fibre by matrix particles (Fig. 2).

The application and study of nylon FRC so far have not been as extensive as for polypropylene FRC, although nylon fibre exhibits good toughness and durability. Wang *et al.* [6] investigated the nylon/cement interface and observed peeling and fibrillation at the fibre surface (Fig. 3). They concluded that the increased interfacial friction during fibre pull-out was due to the increase in surface abrasion.

In this study, the interfacial microstructures and the damage evolution of steel, nylon and polypropylene FRCs were investigated microscopically with scanning electron microscopy (SEM) and energy dispersive X-ray analysis (EDX). Different interfacial damage mechanisms were observed by comparing the interfacial microstructural evolution of the three types of FRC.

2. Experimental procedure

2.1. Specimen and materials

The specimen was a mortar block with an embedded fibre (Fig. 4). Specimen preparation procedures can be found in Leung and Geng [5]. The fibres used included steel wire (low carbon and cold drawn steel), nylon monofilament (Nylon 66) and polypropylene monofilament (relaxed low draw). The steel fibre was 0.5 mm in diameter. The nylon and polypropylene monofilaments (0.5 mm in diameter) were 2143 and 1549 deniers, respectively. The clean surfaces of the virgin fibres are shown in Fig. 5. Mortar was made from Type III Portland cement and mortar sand with a water/cement/sand ratio of 0.5 : 1 : 2. Pull-out tests were performed with saturated surface dry (SSD) specimens at the age of 7 days. The material properties are listed in Table I.

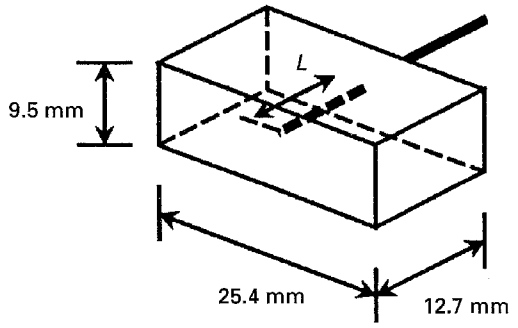

Figure 4 Single-fibre pull-out specimen (embedded length $L = 10$ mm).

2.2. Experimental apparatus

A two-dimensional loading device was designed to perform the fibre pull-out test (Fig. 6). Loads could be applied in two orthogonal directions: the pull-out direction (along the fibre) and the lateral direction (perpendicular to the fibre). The part of the pulled specimen with the embedded fibre was glued to an L-shape specimen holder while the pull-out end of the fibre was held tightly by a grip. The holder and grip were connected to the load cells (Data Instruments) through hardened steel rods. A linear variable differential transducer (LVDT, Lucas Schaevitz) was used to measure the fibre sliding history. The LVDT and its core were mounted on the L-shaped specimen holder and the fibre grip, respectively.

Loading was applied by turning a nut against a reaction block on the end of each loading chain. In the pull-out direction, the nut behind the reaction block was driven by a motor through gears and the loading was displacement-controlled to enable the measurement of post-peak softening behaviour. The loading rate was 0.159 mm min^{-1}. The friction caused by the ball bearing was very small (less than 1.4 N) and was deducted from the results of the pull-out load. In the lateral direction, the nut in front of the reaction block was turned manually to the prescribed lateral compression.

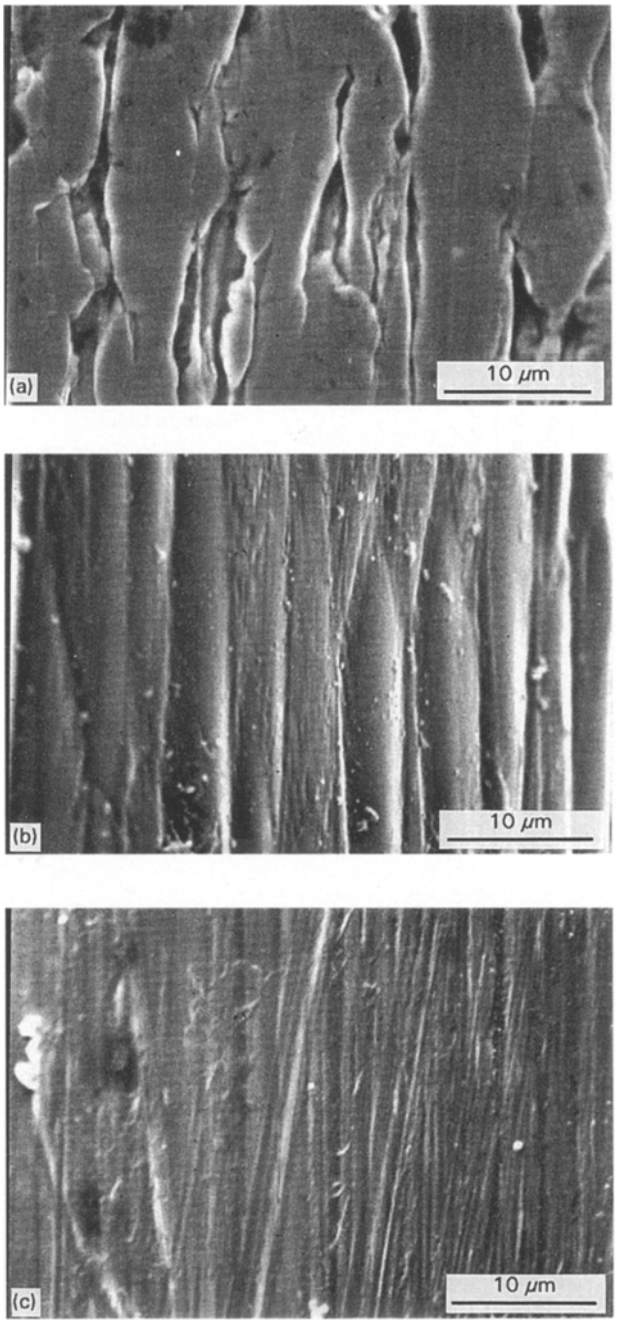

Figure 5 Clean fibre surfaces: (a) steel, (b) nylon, (c) polypropylene.

2.3. Testing procedure

Two sets of specimens were tested with zero lateral compression and a constant lateral compressive stress ($\sigma_c = 20$ MPa). At different stages of pull-out (Fig. 7a), interfacial examinations were carried out (a) before debonding (sliding distance $s = 0$), no pulling is required, (b) immediately after debonding (very small sliding distance), (c) pull-out 1 mm ($s = 1$ mm), (d) pull-out 10 mm ($s = 10$ m). To examine the interface at a given stage, the test was stopped after reaching that particular stage. The tested specimen was then removed from the loading system and split by three-point bending (Fig. 7b) to expose fibre/mortar interfaces. In order to identify the microstructural features of the fibre/mortar interfaces at each stage of pullout, the fibre and mortar groove surfaces were gold-coated for SEM analysis. SEM and EDX were carried out

TABLE I Coefficients of cement mortar and fibers

	Equivalent diameter (mm)	Young's modulus (GPa)	Tensile strength (MPa)	Other strength (MPa)
Cement mortar	–	22.3	3.6 (splitting)	40 (Compres.)
Steel	0.5	200	1242	1040 (yield)
Nylon	0.5	6 [19, 20]	451	–
Polypropylene	0.5	4 [19]	391–462	–

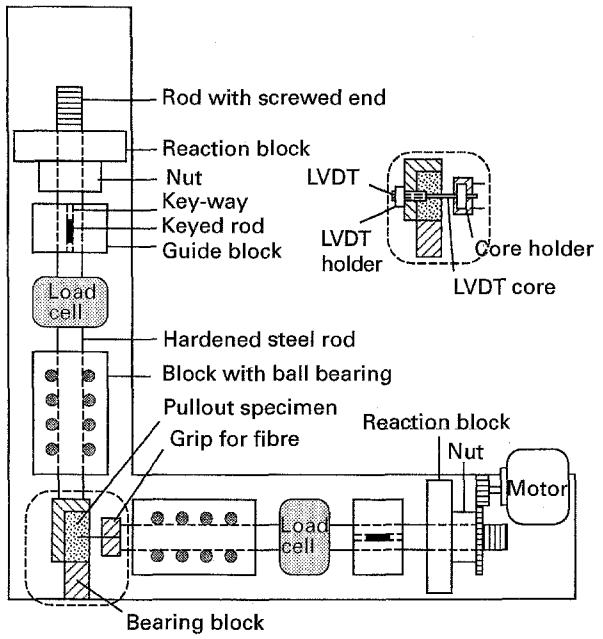

Figure 6 The two-dimensional fibre pull-out device.

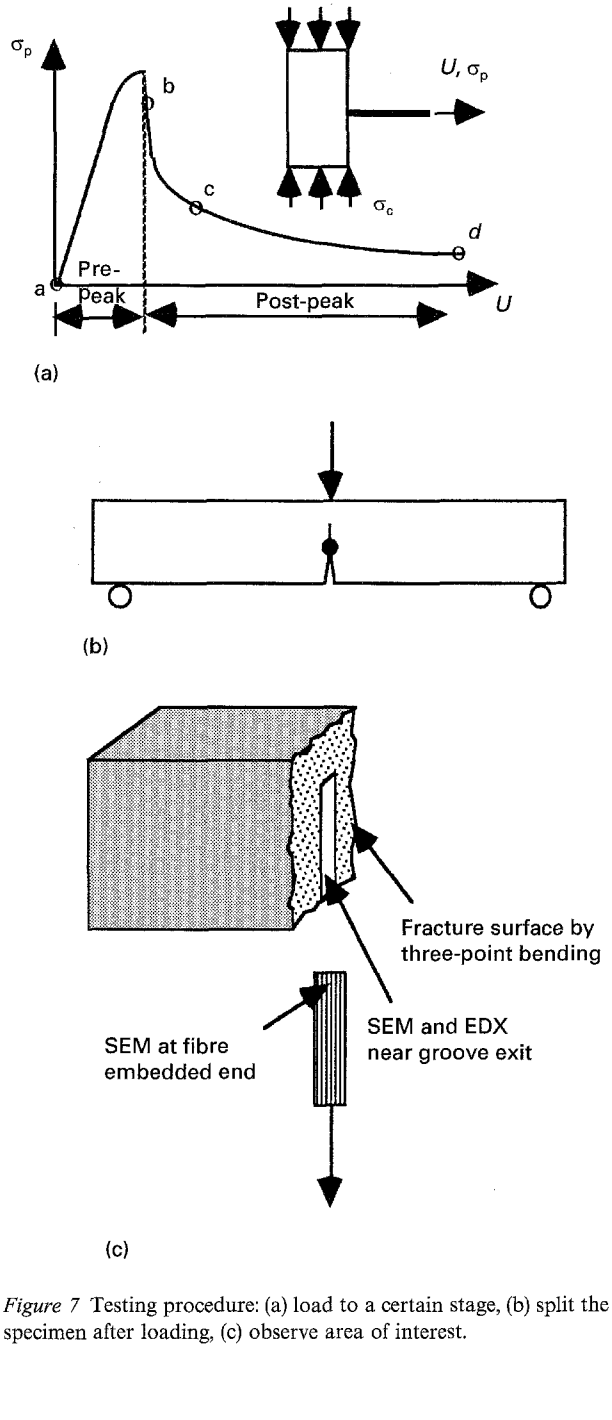

Figure 7 Testing procedure: (a) load to a certain stage, (b) split the specimen after loading, (c) observe area of interest.

near the fibre embedded end and the mortar groove exit, because these locations generally experience the most interfacial interactions (Fig. 7c).

3. Results and discussion

Fig. 8 shows the typical pull-out curves (fibre stress versus displacement at the pulling end of the fibre) for steel, nylon and polypropylene fibres. Compared with the tensile strengths of the fibres (Table I), the peak loads are much lower. Therefore, fibres can be considered within their elastic ranges except that damage may occur at the fibre surface. The post-peak pull-out behaviour shows different trends for different fibres: (a) steel fibre pull-out – decreases rapidly; (b) nylon fibre pull-out – increases slowly; (c) polypropylene fibre pull-out – decreases slowly. With lateral compression, the peak pull-out load increases. However, for the steel fibre, the post-peak load drop also becomes more rapid.

3.1. Steel fibre/mortar interface

Fig. 9 shows the mortar surface when pull-out is under zero lateral compression. Each picture in the figures corresponds to one of the four pull-out stages. At stage (a), the interface is separated by tensile debonding. Most of the mortar surface (Fig. 9a) follows the topology of the steel surface (Fig. 10a). On a very small portion of the surface, cement mortar pieces (CH crystals and C–S–H fibrous blocks) are spalled from the matrix and adhered to the steel surface, similar to the observation of Bentur *et al.* [10] and Pinchin and

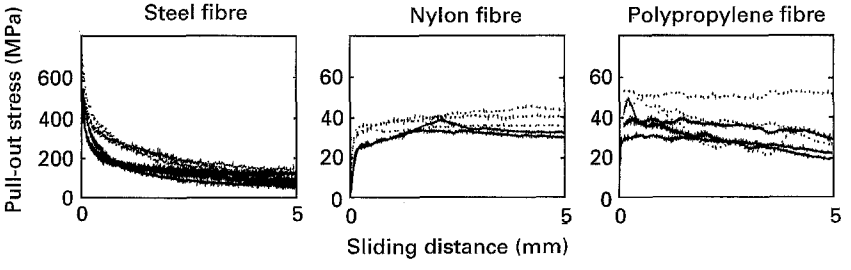

Figure 8 Typical pull-out curves, (—) $\sigma_c = 0$; (···) $\sigma_c = 20$ MPa.

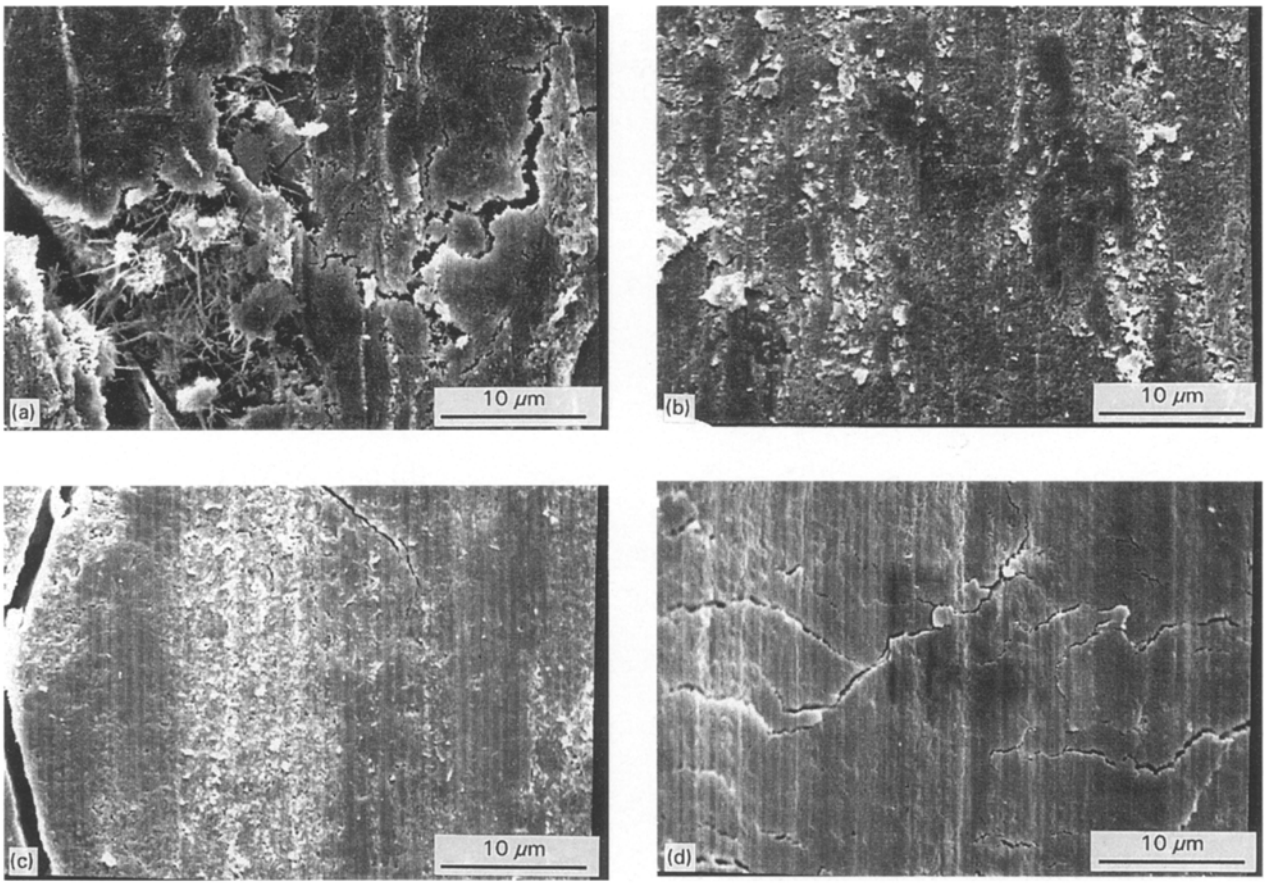

Figure 9 Mortar surface at the steel/mortar interface under no compression ($\sigma_c = 0$). (a) Tensile debonding, (b) shear debonding, (c) pull-out 1 mm, (d) pull-out 10 mm.

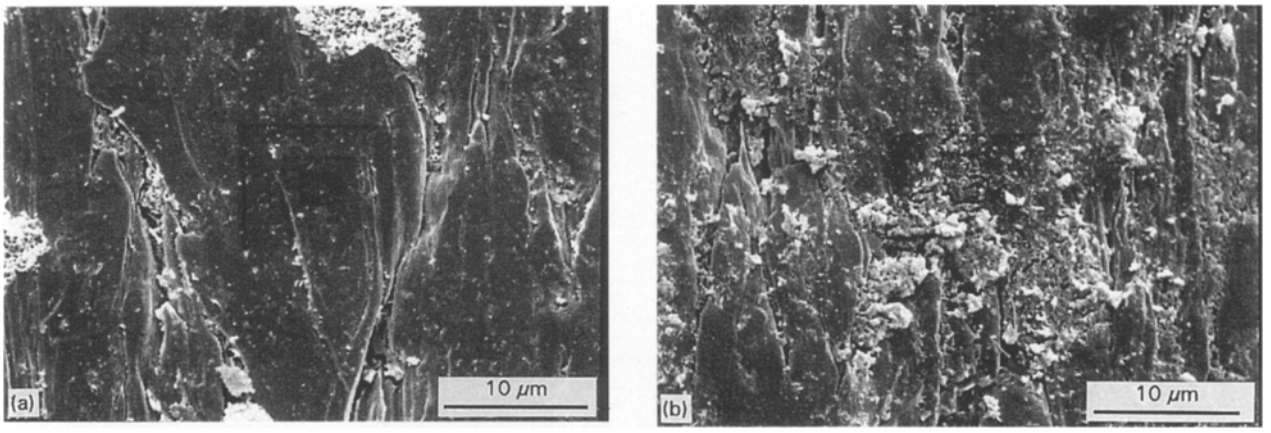

Figure 10 Steel surface at the steel/mortar interface under no compression ($\sigma_c = 0$). (a) Tensile debonding, (b) shear debonding.

Tabor [12]. The result indicates that interfacial fracture usually occurs along the steel/mortar interface, but occasionally occurs within the interfacial transition zone where the tensile strength of the mortar is less than the chemical bond at the interface.

At stage (b), shear debonding can also result in some failure inside the matrix, leading to the presence of mortar particles on the steel surface (Fig. 10b), although most of the debonded surface is on the steel fibre/mortar interface. A small amount of sliding grinds the spalled mortar pieces to small particles of up to 2 μm in size (Figs 9b and 10b).

The irregular spalled mortar pieces are ground to much smaller particles under further pull-out at stages (c) and (d) and become more regular in their shape (Fig. 9c and d). The decrease of particle size is more rapid in the early sliding stage, which agrees well with the rapid initial decrease of the post-peak pull-out curves. At the final stage (d), both the mortar surface and the steel surface (Figs 9d and 11a) are smoothed. On the mortar surface, cracks are filled with very fine particles and only the scratch lines can be observed. The steel surface experiences plastic yielding during fibre pull-out, similar to the observation of Banthia *et al.* [21].

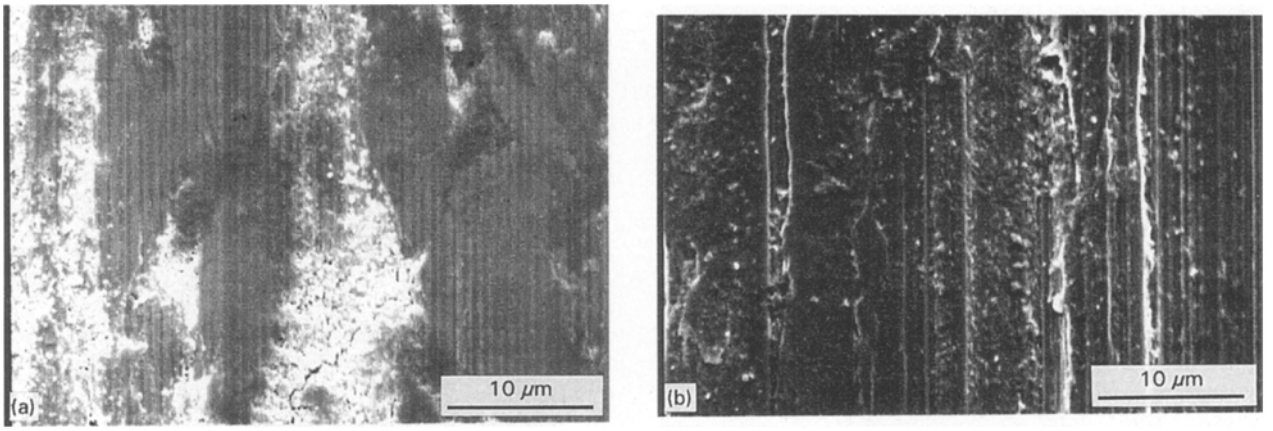

Figure 11 Steel surface at the steel/mortar interface at Stage (d), 10 mm pull-out. (a) $\sigma_c = 0$, (b) $\sigma_c = 20$ MPa.

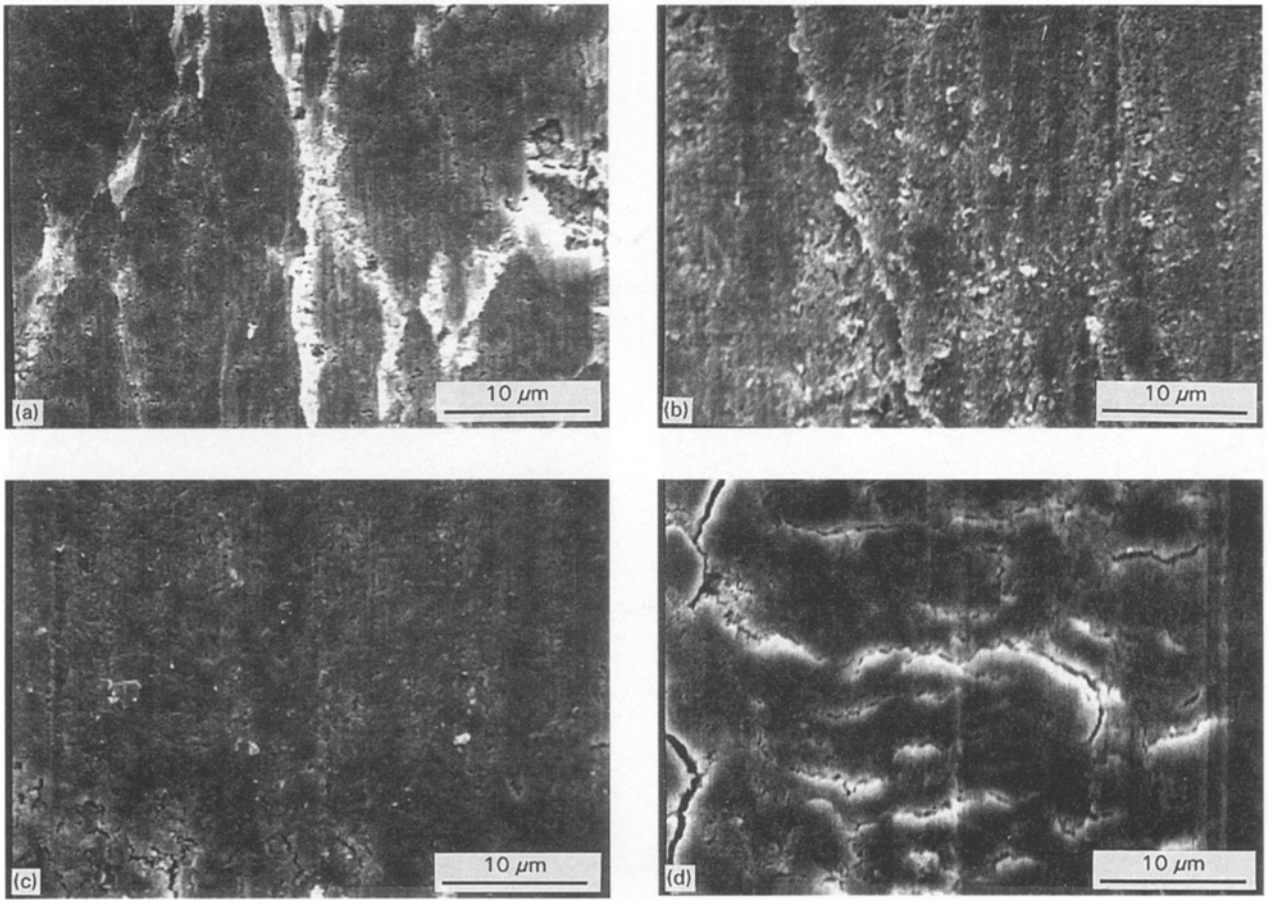

Figure 12 Mortar surface at the steel/mortar interface under compression ($\sigma_c = 20$ MPa). (a) Tensile debonding, (b) shear debonding, (c) pull-out 1 mm, (d) pull-out 10 mm.

The same observation is repeated for the case with lateral compression (Fig. 12). At stage (a), surface compaction due to compression can be observed in a small portion of the surface (white spots). By comparison of the mortar surface at stages (b) and (c) for the cases with and without compression in Figs 9 and 12, one can observe that the particle size decreases more rapidly when compression is applied. The lateral compression accelerates the abrasion process due to severe grinding. At stage (d), the steel surface exhibits scratch lines (Fig. 11b) which indicates more surface yielding.

In order to quantify the surface damage, energy dispersive X-ray analysis (EDX) was carried out. Because the mortar surface was relatively smooth and the analysed area was roughly 0.06 mm^2, the EDX analysis could provide reasonable results. Fig. 13 shows a typical X-ray spectrum. From the ratio of the area under the calcium and silicon peaks on the X-ray spectrum, one can deduce the change in CH/C–S–H

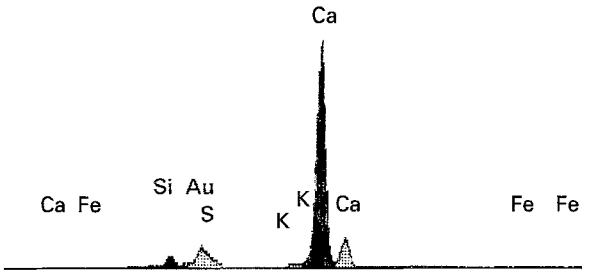

Figure 13 X-ray spectrum.

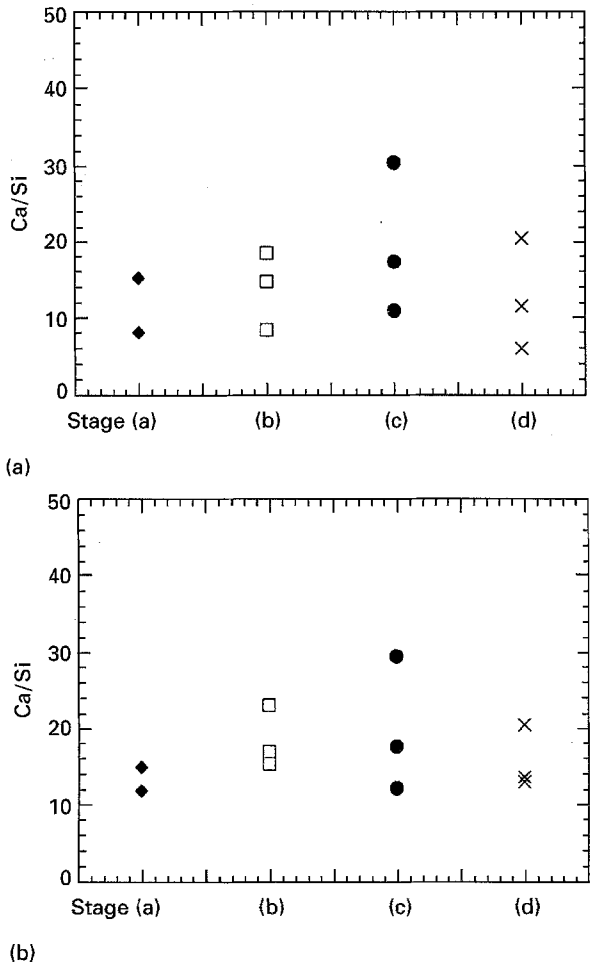

Figure 14 Ca/Si ratio at the mortar surface of steel/mortar interface, (a) $\sigma_c = 0$, (b) $\sigma_c = 20$ MPa: (◆) before debonding, (□) after debonding, (●) pull-out 1 mm, (×) pull-out 10 mm.

on the matrix surface during the fibre debonding/pull-out process. The areas are calculated by first removing the effect of the background and the neighbouring peaks. Fig. 14 shows the Ca/Si ratio at the four pull-out stages for mortar surface. The Ca/Si ratio at the steel/mortar interface increases in the first three stages and decreases at the last stage. Based on the SEM observations in Figs 9 and 12, there are two possible contributions to the increase and the decrease:

(a) debonding occurs preferentially in the weak area at the interface or in the matrix, where the brittle CH phase is rich. In the early pull-out stages, the brittle CH phase may be crushed when it interacts with the steel surface and is smeared over the matrix surface, leading to an increase in the Ca/Si ratio;

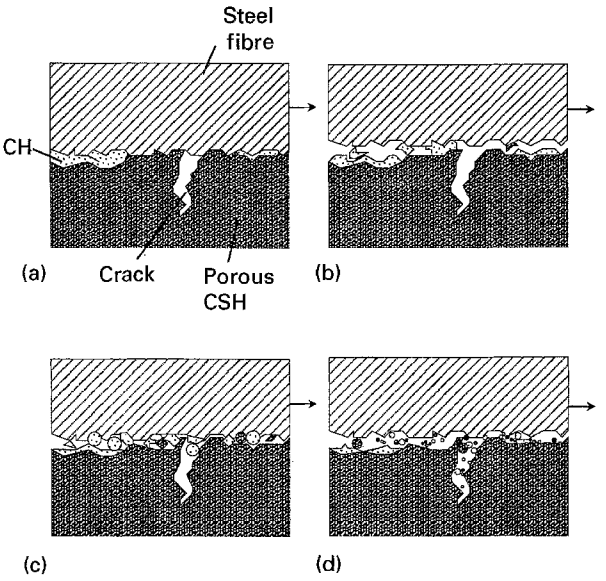

Figure 15 Damage Evolution at the steel fibre/mortar interface: (a) before debonding, (b) debonding, (c) pull-out (short distance), (d) pull-out (long distance).

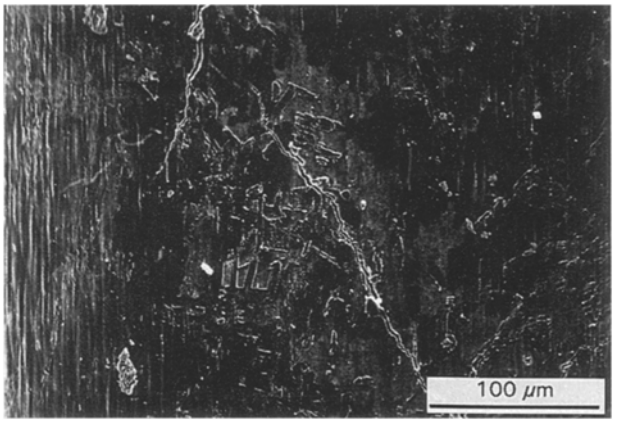

Figure 16 Mortar surface at the nylon fibre/mortar interface.

(b) the decrease of the Ca/Si ratio can be attributed to abrasion. On further fibre sliding, the crushed CH phase is ground into much finer particles and partly swept into the pores and cracks on the mortar surface, hence exposing the underlying C–S–H phase. This process can reduce the calcium count and increase the silicon count.

One can see in Fig. 14 that debonding and an inevitable small amount of sliding at stage (b) increases the Ca/Si ratio. Further sliding to stage (c) leads to crushing and smearing of the CH phase, which increases the Ca/Si ratio. After very long sliding distance (stage d), sweeping and cleaning of the CH phase occurs, thus decreasing the Ca/Si ratio.

The results of EDX cannot be explained by the surface compaction mechanism proposed by Pinchin and Tabor [12]. In Fig. 14, the Ca/Si ratio remains the same for the cases both with and without compression at stage (a). Because the fibre is not pulled at stage (a) and no abrasion can take place, one can conclude that surface compaction will not alter the Ca/Si ratio. Nevertheless, the Ca/Si ratio during fibre sliding varies significantly for cases both with and without

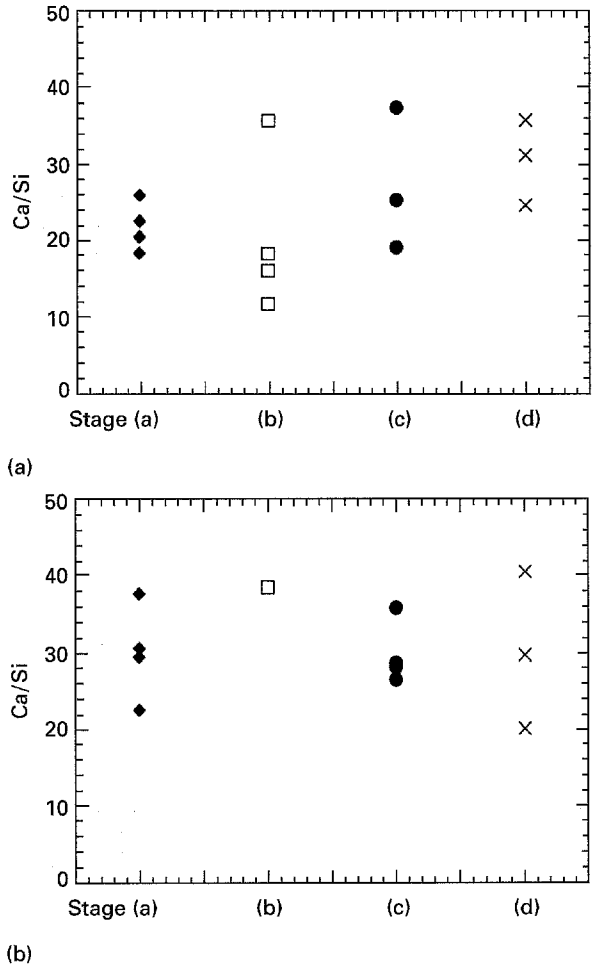

Figure 17 Ca/Si ratio at the mortar surface of nylon/mortar interface, (a) $\sigma_c = 0$, (b) $\sigma_c = 20$ MPa: (◆) before debonding, (□) after debonding, (●) pull-out 1 mm, (×) pull-out 10 mm.

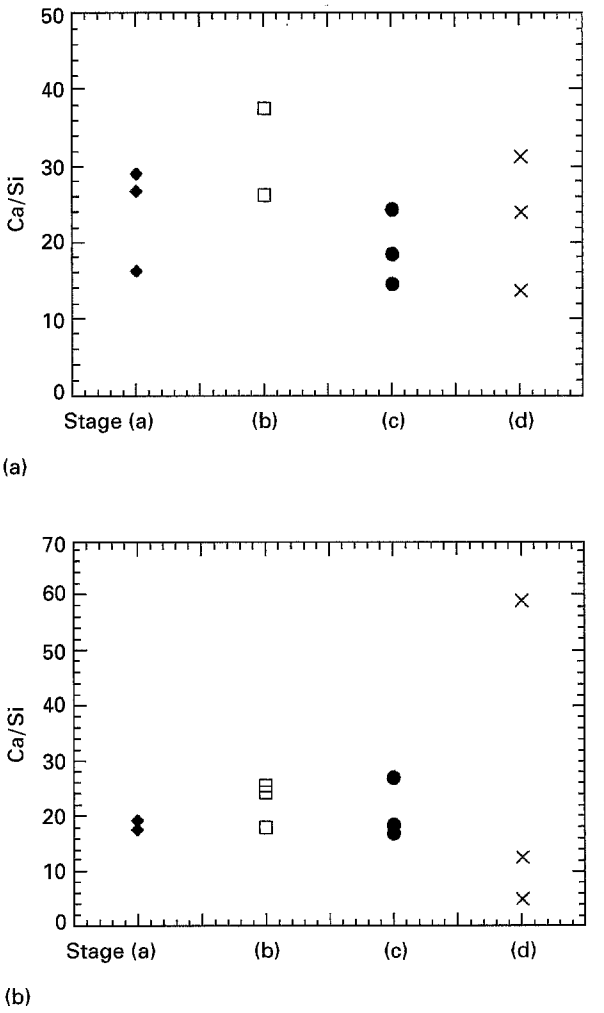

Figure 18 Ca/Si ratio at the mortar surface of polypropylene/mortar interface. (a) $\sigma_c = 0$, (b) $\sigma_c = 20$ MPa: (◆) before debonding, (□) after debonding, (●) pull-out 1 mm, (×) pull-out 10 mm.

compression, which confirms that the surface microstructures changes significantly during fibre sliding. This microstructural evolution is caused by the surface grinding and abrasion.

Based on microscopic observation and EDX analysis, the pull-out process can be characterized by a simple model in Fig. 15. Brittle CH crystal is first abraded followed by abrasion of C–S–H gel. This process results in a change of Ca/Si ratio on the surface due to the grinding and sweeping of CH phase into pores and cracks.

3.2. Polymeric fibre/mortar interface

Unlike the steel/mortar interface, the mortar surfaces at the nylon/mortar and polypropylene/mortar interfaces show little damage (Fig. 16), similar to the observation of Chan and Li [22]. The EDX analysis shows no trend of Ca/Si variation (Figs 17 and 18), which indicate that the interfacial transition zone is intact. Similar to the observations of Pinchin and Tabor [6] and Baggott and Gandhi [16], the polymeric fibre surface experiences peeling, especially at the fibre embedded end or over a long sliding distance. The data scattering of the Ca/Si ratio for polypropylene fibre under compression at stage (d) (Fig. 18b) is consistent with randomness of the pull-out curves at long sliding distance (Fig. 8).

During mixing of nylon FRC, cement particles can penetrate into the rough surface of the nylon fibre to form a hydrogen bond. The hardened mortar can either tear away some of the nylon surface or spall from the matrix and adhere to the fibre. The low asperity polypropylene fibre has less peeling because of the weaker van der Waals bonds at the interface. After total debonding, the stiffer mortar surface causes surface peeling in both nylon fibre (Fig. 19a) and polypropylene fibre (Fig. 20a). For both nylon and polypropylene fibre FRCs, friction plays a dominant role in the interfacial resistance.

Because nylon fibre is hydrophilic, water may penetrate into the nylon surface and causes fibre swelling. The increase of the fibre radius due to peeling and swelling causes a significantly higher interfacial compression and increases the post-debonding load over sliding distance. On the other hand, the polypropylene fibre is hydrophobic. The surface is ploughed with long whiskers and the long scratch lines. The scratch lines (Fig. 20a) are similar to those on the steel fibre surface caused by surface hardening. The lower surface asperity of the polypropylene fibre results in the post-debonding decrease and randomness of pull-out load.

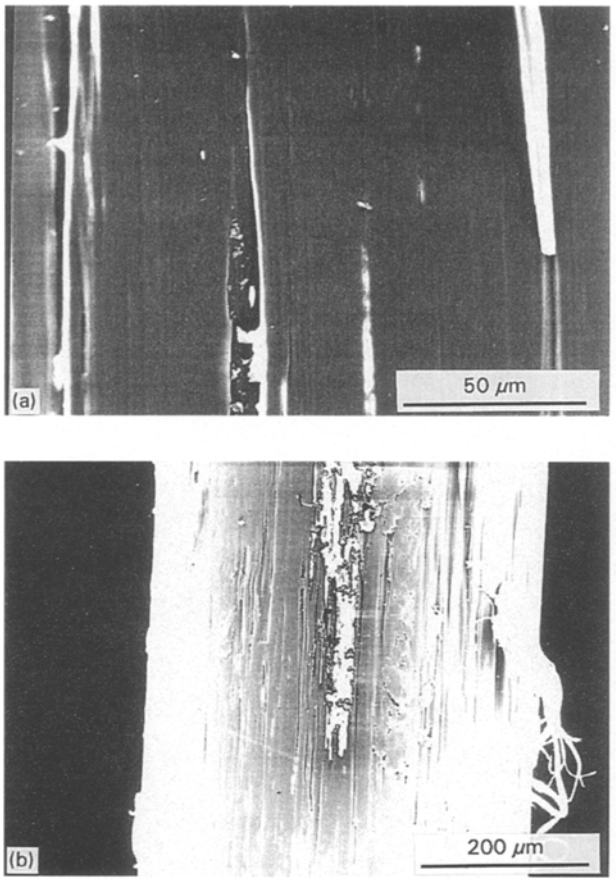

Figure 19 Nylon surface (pull-out 10 mm). (a) $\sigma_c = 0$, (b) $\sigma_c = 20$ MPa.

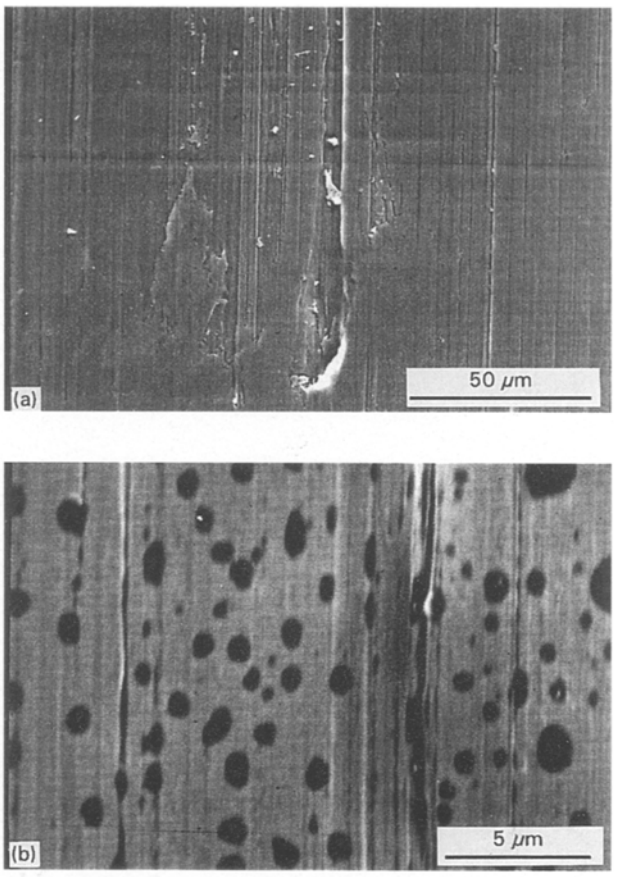

Figure 20 Polypropylene surface (pull-out 10 mm). (a) $\sigma_c = 0$, (b) $\sigma_c = 20$ MPa.

When the fibre is pulled under compression over a long distance (10 mm), severe peeling and shaving are observed on the nylon fibre surface (Fig. 19b) and black holes are observed on the polypropylene surface (Fig. 20b). These black holes are similar to those observed on a thin polymer film failed in tension. The polypropylene fibre surface is subjected to shear load by the mortar matrix (surface stretch microscopically) during pull-out. Under the low pulling rate and the long pull-out distance, the fibre surface undergoes significant molecular alignment and creeping which results in a pseudo volumetric increase. In order to maintain a constant volume, small holes are generated by the Poisson's effect, i.e. the surface ligaments get thinner and break into small holes.

4. Conclusions

The microstructural features of the steel, nylon and polypropylene fibre/mortar interfaces during fibre debonding and pull-out have been studied. Mortar abrasion was found to be a major mechanism accounting for damage at the steel fibre/mortar interfacial zone. The damage at the nylon and polypropylene fibre/mortar interfaces was mainly due to fibre surface peeling while the mortar surface experiences very little damage. On applying lateral compression to the mortar during fibre pull-out, the abrasion effect became more severe for steel fibres. In both nylon and polypropylene, peeling became more significant and holes could form on the polypropylene surface.

Acknowledgements

The authors thank Dr Yiping Qiu and Professor Stanley Becker, Department of Mechanical Engineering, MIT, for their illuminating discussions.

References

1. S. P. SHAH and C. OUYANG, *J. Am. Ceram. Soc.* **74** (1991) 2727.
2. A. BENTUR and S. MINDESS, "Fiber Reinforced Cementitious Composites" (Elsevier, New York, 1990).
3. V. C. LI and C. K. Y. LEUNG, *ASCE J. Eng. Mech.* **118** (1992) 2228.
4. A. E. NAAMAN and S. P. SHAH, *ASCE J. Struct. Div.* **102** (ST8) (1976) 1537.
5. C. K. Y. LEUNG, and Y. GENG, in "Interface Fracture and Bond", ACI SP-156, edited by O. Buyukozturk and M. Wecheratana (1995) p. 153.
6. Y. WANG, V. C. LI and S. BACKER, in Materials Research Society Proceedings **114**, "Bonding in Cementitious Composites", edited by S. Mindess and S. P. Shah, (MRS. Pittsburgh, PA, 1988) p. 159.
7. S. MINDESS, in "Materials Science of Concrete I", edited by Jan P. Skalny (American Ceramic Society, Westerville, OH, 1989) p. 163.
8. D. J. PINCHIN and D. TABOR, *Cem. Concr. Res.* **8** (1978) 15.
9. M. N. AL KHALAF and C. L. PAGE, *ibid.* **9** (1979) 197.
10. A. BENTUR, S. DIAMOND and S. MINDESS, *J. Mater. Sci.* **20** (1985) 3610.

11. S. WEI, J. A. MANDEL and S. SAID, *ACI J.* (1986) 597.
12. D. J. PINCHIN and D. TABOR, *J. Mater. Sci.* **13** (1978) 1261.
13. I. SOROKA and P. J. SEREDA, in "Proceedings of the 5th International Symposium on the Chemistry of Cement", Vol. 3 (Tokyo, 1968) p. 67.
14. D. J. HANNANT, "Fiber Cements and Fiber Concretes" (Wiley, New York, 1978).
15. N. J. DAVE and D. G. ELLIS, *Int. J. Cem. Compos.* **1** (1978) 19.
16. R. BAGGOTT and D. GANDHI, *J. Mater. Sci.* **16** (1981) 65.
17. E. K. RICE, G. L. VONDRAN and H. O. KUNBARGI, in Materials Research Society Proceedings **114**, "Bonding in Cementitious Composites", edited by S. Mindess and S. P. Shah (MRS, Pittsburgh, PA, 1988) p. 145.
18. A. PELED, H. GUTTMAN and A. BENTUR, *Cem. Concr. Compos.* **14** (1992) 277.
19. P. N. BALAGURU and S. P. SHAH, "Fiber Reinforced Cement Composites" (McGraw-Hill, New York, 1992) p. 108.
20. R.W. MONCRIEFF, "Man Made Fibers", 6th Edn (Wiley, New York, 1975) p. 653.
21. N. BANTHIA, J. -F. TROTTIER, M. PIGEON and M.R. KRISHNADEV, in "High Performance Fiber Reinforced Cement Composites", edited by H.W. Reinhardt and A.E. Naaman, (Spon, London, 1992) p. 456.
22. Y. -W. CHAN, and V. C. LI, in "Proceedings of the 1st International Conference on Composite Engineering" edited by D. Hui (1994) p. 293.

Received 22 December 1994
and accepted 2 May 1995